ACS Electrochemistry

Open Access

pubs.acs.org/electrochem

Article

Potential Gradient Effects on Electron Transfer Reactions Mediated by Quantum Capacitive States

Yuliana Pérez Sánchez, Adriano dos Santos, and Paulo Roberto Bueno*

Cite This: ACS Electrochem. 2025, 1, 832−841

Read Online

ACCESS | Metrics & More | Article Recommendations | Supporting Information

ABSTRACT: This study investigates the effect of the potential gradient on electron transfer (ET) reactions occurring in redox-active monolayers self-assembled on metallic electrodes. Redox centers within the monolayer serve as quantum capacitive (C_q) energy levels ($E = e^2/C_q$) that mediate ET from free redox couples (in the electrolyte) to the electrode. Different from diffusion-controlled ET reactions where the current collector forms a junction with the free redox couples, C_q-mediated ET reactions are diffusionless and hence exhibit quantized resistance limits of $R_q \propto h/e^2 \sim 25.8$ kΩ that follows quantum electrodynamics principles. This diffusionless ET dynamics relies on the energy level alignment with the redox molecules of the monolayer and electrolyte environment that ultimately governs the ET rate dynamics with a rate constant of $\nu \propto e^2/hC_q \propto 1/R_qC_q$. Changes in the acidity (inducing potential gradient) of the redox-active monolayer due to the deprotonation of free Fc−COOH redox-couple groups significantly impact the charging behavior of the $E = e^2/C_q$ states, thus affecting the energy alignment between anchored and free redox species. That the acidity of the monolayer affects C_q-mediated ET efficiency is a piece of valuable information for designing suitable energy alignment between man-made C_q interfaces and redox couples present in electrolytic solvents.

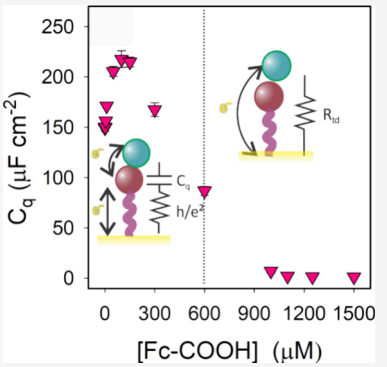

KEYWORDS: *charge-transfer mediation, potential gradient effects, diffusionless electron transfer reaction, quantum electrodynamics, quantum capacitance, conductance quantum, quantum electrochemistry*

INTRODUCTION

In general, heterogeneous electron transfer (ET) reactions are mass-transport-dependent processes in which electroactive species (donor or acceptor moieties) diffuse at the electrode surface and undergo redox ET reactions. The dynamics of the reaction can be investigated by monitoring the electric current i response as a function of the potential scan rate $s = dV/dt$ perturbation that predictability follows a Randles−Sevcik diffusional control,[1] in which $i \propto s^{1/2}$. In contrast, diffusionless ET reactions follow $i \propto s$ rather than $i \propto s^{1/2}$, constituting a charge dynamics between an electrode and chemically attached redox species with measurable C_q and energy $E = e^2/C_q$ states (where e is the elementary charge of the electron) that lead to[2] $i = C_q s$ (where C_q is straightly identified as the constant of proportionality between i and s).

This ET dynamics, which occurs without a diffusion control, is referred to as diffusionless ET reactions and governed by quantum electrodynamics principles in which the rate ν of ET follows the $\nu \propto e^2/hC_q \propto E/h$ relationship (where h is Planck's constant). This C_q-based rate constant of $\nu \propto e^2/hC_q$ comprises the Marcus ET rate constant whether statistical thermodynamics is considered over E with a Boltzmann approximation[3] of the state occupancy. Diffusionless reactions have been studied at electroactive interfaces comprising redox-active species self-assembled over metallic electrodes[4,5] (referred to as redox-SAMs), but only recently have they been noted to follow quantum electrodynamics principles within the quantum-rate theory.[3]

Quantum-rate theory[3] has been applied to study the electronic structure of graphene[6] and quantum dots[7] and to study the dynamics of electrochemical reactions occurring in redox-SAMs,[8,9] permitting a better understanding of diffusionless ET dynamics settings that comply with Laviron's approach,[8] which predicts $i \propto s$. Additionally to comply with the classical $i \propto s$ relationship, it has been demonstrated that the transmittance probability of the electron involved with reactions within redox-SAMs is directly associated with the resistance quantum $R_q \propto h/e^2$[10] and $C_q = e^2(dn/dE)$, where dn/dE is the density-of-states (DOS) that correlates with the electronic structure of the monolayer. In particular, the relationship between electron's transmittance, associated with R_q, and the electronic structure, associated with C_q, has a characteristic time-constant $\tau = R_qC_q$ that governs the rate $\nu = 1/\tau = E/h$ with which ET occurs.

Received: September 30, 2024
Revised: April 12, 2025
Accepted: April 14, 2025
Published: April 29, 2025

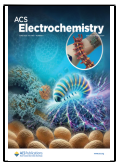

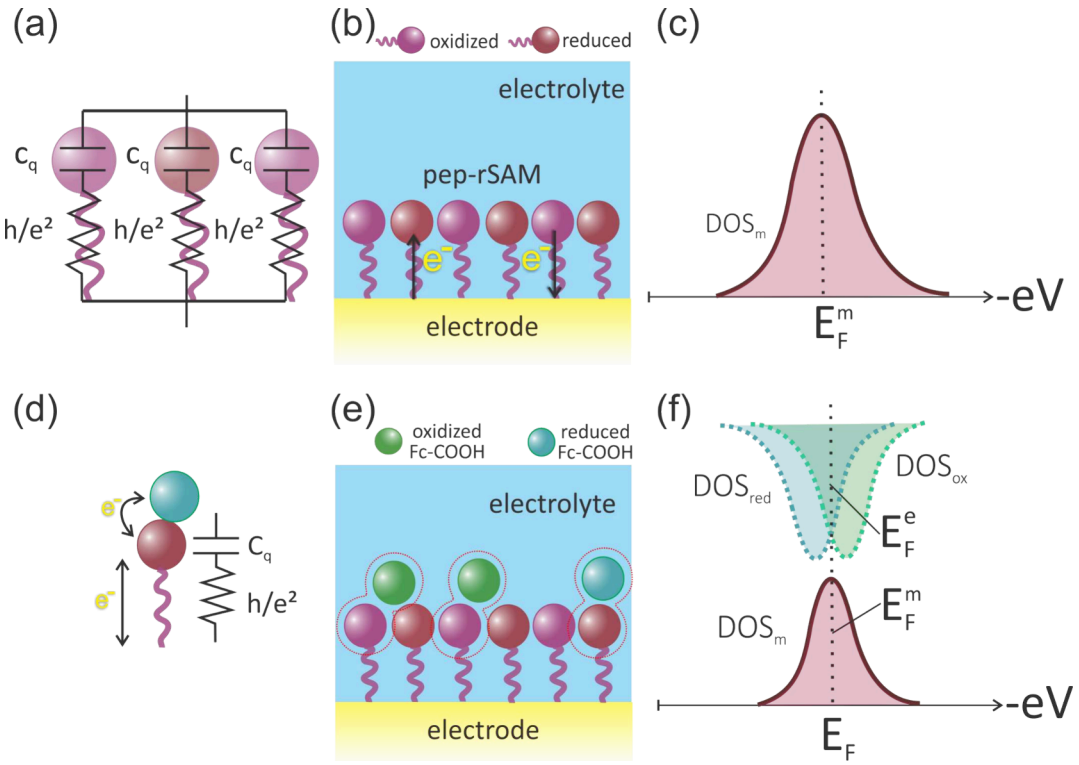

Figure 1. Schematic representation of the pep-rSAM in an electrolyte environment and its role in mediating the ET reaction between the electrode and Fc−COOH in solution. (a) Each redox peptide constituting the SAM acts as individual quantum states, with $r_{q_i} = h/e^2$ and c_{q_i} arranged in series, and each $r_q c_q$ time-constant is arranged in parallel to another. The measurable average time-constant is $R_q C_q$ of diffusionless ET dynamics. (b) In this ET reaction dynamics, charge carrier occupancy occurs within the average C_q states of the ensemble depending on the reduction or oxidation state of the pep-rSAM, obeying eq 1. (c) The electronic structure (or density-of-states) of pep-rSAM follows a Gaussian-like distribution, where at formal potential energy E_F^m, half of the C_q states are oxidized and the other half are reduced. (d) Illustration of the mediation of ET reaction by C_q states, where a two-step ET event is likely to occur owing to the mediation phenomenon in which ET occurs through C_q with the free Fc−COOH state. (e) Schematic of the diffusionless ET dynamics mediated by C_q states. (f) Overlap between C_q and free Fc−COOH states in electrolytic medium enhanced with the alignment between formal potential energy states E_F, i.e., when $E_F^m = E_F^e$, where m refers to monolayer and e to the electrolyte.

This quantum mechanical resistive-capacitive time-constant τ, measurable in redox-SAMs, has been previously identified as $R_{ct}C_{ads}$ by Creager and colleagues,[11] where R_{ct} is referred to as the charge-transfer resistance and C_{ads} as a pseudo-capacitance associated with the irreversible adsorption (ads) of the redox species over the electrode. Note that the quantum-rate $\nu \propto 1/\tau$ is proportional to the reciprocal of the characteristic $\tau = R_q C_q$ constant and, hence, it encompasses Creager's description of $\tau = R_{ct}C_{ads}$ as a particular setting of the quantum-rate theory. This is owing to R_{ct} being proved to be quantized, i.e., proportional to R_q in the ET reaction dynamics of redox-SAMs, as demonstrated in ref 9. On the other hand, the meaning of C_q within the quantum-rate theory is broader than that proposed by Creager (as a type of adsorption capacitance associated with the redox molecular coverage), as it not only encompasses ET dynamics of redox-SAMs but also describes non-redox (where ET reaction is absent) quantum electrodynamics processes within graphene,[6] quantum dots,[7] and reduced graphene oxide structures[12] where, in the latter, it is able of explaining the supercapacitance within this type of carbonaceous structure.[12]

By applying statistical mechanics over $\nu = E/h \propto e^2/hC_q$ to describe the dynamics of redox-SAMs at finite (room) temperature, each molecule over the SAM, fabricated over the electrode, has a time-constant $\tau_i = r_{q_i}c_{q_i}$ that describes its dynamics within the ensemble average value of $\tau = R_q C_q$, as depicted in Figure 1a. The electron's occupancy of the states within the ensemble is associated with the reduction or oxidation state of the SAM, following the Fermi−Dirac statistics $f = [1 + \exp(E/k_BT)]^{-1}$, where k_B is the Boltzmann constant and T is the temperature. $E = \mu - E_F^m$, where μ is the chemical potential energy of the electrons modulated by the potential imposed by the potentiostat to the electrode and E_F^m is the formal potential energy of the redox-active species contained in the redox-SAM (Figure 1b). Note that whenever μ equates to E_F^m, the electron's occupancy of the redox-SAM is half, i.e., $f = 1/2$. This $f = 1/2$ occupancy signifies that the net electric current flowing in the interface is null and referred to as exchange current, where there is an equilibrium occupancy in which half of the states are reduced and half are oxidized, implying that reduction and oxidation currents are equal and flowing in opposite directions,[10] and a DOS_m is measurable through measuring C_q, as illustrated in Figure 1c.

Owing to C_q being associated with the DOS,[13] its measurement permits inference of the electronic structure occupancy, as shown in previous studies.[6,14,15] Regarding redox-SAMs, the DOS converts into a Gaussian-like shape, Figure 1c, that is essentially controlled by the $f(1-f)$ term of a thermally broadened capacitive function, such as

$$C_q = \frac{e^2 N}{k_B T} f(1-f) \tag{1}$$

https://doi.org/10.1021/acselectrochem.4c00112
ACS Electrochem. 2025, 1, 832−841

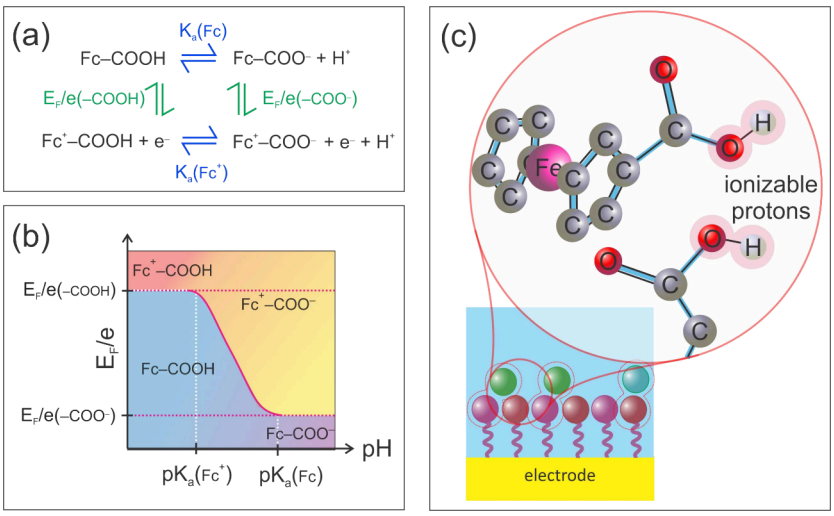

Figure 2. (a) Square-scheme mechanism of the PCET reaction for Fc−COOH in aqueous solvent. Vertical and horizontal equilibrium arrows represent the individual electron and protonation/deprotonation steps, respectively, and the corresponding acid dissociation constants, K_a, and formal potentials, E_F/e, are shown. (b) Pourbaix diagram plotting E_F/e versus pH; the solid line separates the oxidized and reduced species, whereas dotted vertical lines delimit the regions of protonated and deprotonated species. The intersections of the solid and dotted line indicates the pK_a values. (c) The proton-ionizable groups of the redox-tagged peptide and free Fc−COOH (ET-mediating setting shown in Figure 1e).

where N is the total amount of accessible quantum states. The modification of an electrode with a redox-SAM hence introduces accessible redox-active state levels $E = e^2/C_q$, permitting ET dynamics to be mediated by C_q states where ET dynamics between free redox and electrode states occurs in a diffusionless manner following $i = C_q s$ dependence, as depicted in Figure 1d. In the latter type of diffusionless ET dynamics, C_q-mediating states play a pivotal role in facilitating diffusionless redox reaction dynamics from the electrode to the free redox states (and vice versa) in the electrolyte, as illustrated in Figure 1e,f. In other words, the presence of C_q states in the electrode suppresses the diffusion dependence $i \propto s^{1/2}$ of ET reactions that occur in the absence of C_q states in the electrode, e.g., in the case in which there is a direct contact between free redox species in the electrolyte and a non-modified metallic electrode.

ET mediation through C_q states is achieved because of the suitable energy alignment between $E = e^2/C_q$ and the free redox states in the electrolyte.[10] $-eV = \mu - E_F^m$, where V is the potential difference of the potentiostat applied to the working electrode in respect to the reference, whether μ equates to E_F^m; hence, $f = 1/2$ and C_q is maximum, as predicted by eq 1. The energy alignment in the interface can additionally involve the free redox energy states E_F^e, as illustrated in Figure 1f. In the latter settings, the energy alignment between E_F^e and E_F^m allows quantum ET dynamics, where diffusion control is absent. Figure 1f illustrates the alignment between the redox DOS (DOS_{ox} and DOS_{red}), formal potential energy E_F^e of free the redox moieties in the electrolyte (commonly referred to as Marcus−Gerischer redox DOS in the electrochemical nomenclature of the literature[1]), and E_F^m of the monolayer. The alignment between these energy levels E_F (physicists refer to this as the Fermi level)[16] can be tested, complementary to impedance measurements, using cyclic voltammetry, in which the overlap of these redox processes can be noticed, as reported in ref 10.

ET requires a significant energy barrier without mediation by capacitive DOS states, which results in increased resistance (represented by R_{td}, which settles in parallel to the quantum RC branch within a characteristic time-constant $\tau = R_q C_q$). This resistance is associated with the "diffusive" transfer of electrons directly from redox species in the solution phase to the electrode.[10] R_{td} corresponds to the charge-transfer resistance R_{ct} observed in a typical electrode reaction using unmodified or bare Au (metallic) electrodes, which characterizes a diffusion-controlled reaction.[17]

Note that C_q is the experimental variable required for determining the ET rate constant and can be measured using time-dependent approaches, such as electrochemical impedance spectroscopy (EIS).[18] The details of the quantum-rate theoretical prediction of the rate constant $\nu = E/h$ (from now on named as k for agreement with electrochemistry's nomenclature) for the heterogeneous ET reaction in a diffusionless regime are introduced in Section SI.1 (of the Supporting Information), permitting access to the electrodynamics or kinetics through the measurement of C_q since $k = 4(e^2/hC_q)$,[8] where C_q is the only experimental variable.

The occupancy of quantum capacitive states is sensitive to environmental changes,[19] such that diffusionless interfacial ET dynamics is influenced by factors such as the dielectric characteristics of the environment, T, and electronic coupling between the donor and acceptor states.[20−22] The acidity/basicity of the molecular moieties influences the ET reaction and formal potential E_F^m/e of the redox-SAM, resulting in the pH-dependent formation of charged interfaces or redox species within the SAM.[23−28]

Proton transfer can occur when coupled with ET reactions, known as proton-coupled electron transfer (PCET) reactions. These concerted (not necessarily synchronous) transfers of electrons and protons (H^+) are significantly influenced by solvent properties.[29] For example, protic solvents actively participate in the PCET reaction by accepting protons owing to their ability to form hydrogen bonds.[30] This stabilizes the H^+ intermediate and significantly affects the reaction kinetics compared with aprotic solvents, where the kinetics are primarily governed by redox species with ionizable proton groups.[31]

https://doi.org/10.1021/acselectrochem.4c00112
ACS Electrochem. 2025, 1, 832−841

Figure 2a shows the PCET schematic reaction of ferrocene carboxylic acid (Fc−COOH) with a strong carboxylic acid group (as well as that of $Fc(CH_2)_nCOOH$ at $n \geq 1$). Fc−COOH readily undergoes deprotonation because of intramolecular charge stabilization by the electrostatic effect.[23] The square-scheme mechanism for the PCET reaction of Fc−COOH is shown in Figure 2a, as depicted in the Pourbaix diagram for a single electron−proton (e^-/H^+) dynamics of Fc−COOH, as schematically denoted in the bottom of Figure 2b. This Pourbaix diagram indicates regions where the oxidized/reduced protonated (Fc^+−COOH/Fc−COOH) and deprotonated (Fc^+−COO^-/Fc−COO^-) species are evident, and it can be noted that at the extremes of the pH axis, the E_F/e redox is pH-independent (horizontal solid lines). On the other hand, between $pK_a(Fc^+)$ and $pK_a(Fc)$ (sloping region), the E_F/e is pH-dependent, and it determines the pH region in which PCET is prominent.[31]

Electrochemical analysis of Fc−COOH in 100 mM tetrabutylammonium perchlorate in 4:1 (v/v) acetonitrile/water, where pH is adjusted using organic base and inorganic acid, permits the measurement of the oxidation and reduction acid dissociation constants of $pK_a(Fc^+) \sim 4.5$ and $pK_a(Fc) \sim 7.8$, respectively. E_F/e for both forms was measured as $E_F/e(-COO^-) \sim 337$ mV and $E_F/e(-COOH) \sim 528$ mV.[23]

The sigmoidal dependence of the E_F/e and pK_a is due to a Nernstian behavior in which the concentrations of reduced and oxidized species are correlated with the pK_a, as detailed in Section SI.3. A correlation with the quantum-rate theory can be established by noting that the energy alignment between E_F^m/e and E_F^e/e is influenced by Fc/Fc^+ species involved in the PCET equilibrium reaction, which can be quantified in terms of the Fermi−Dirac distribution function, where $-e\Delta V = (\mu - E_F^m)$ is stated as

$$-\Delta V = \frac{1}{e}(\mu - E_F^m) = \frac{k_B T}{e} \ln\left(\frac{f}{1-f}\right) \quad (2)$$

with f corresponding to reduced states of the redox-SAM, whereas $1 - f$ corresponds to the oxidation. Hence, according to eq 1, changes in $[H^+]$ influence redox state occupancy and, consequently, the E_F^m/e and C_q of the redox-SAM and the energy alignment with E_F^e/e. Thus, the ET dynamics (in the present case governed by quantum electrodynamics principles) is influenced by the charge state of the redox-SAM that is, in turn, affected by $[H^+]$ associated with the PCET reaction, as will be demonstrated further here.

The ET mediation discussed above[10] involves an electroactive interface with hydrogen-ionizable moieties near the redox sites (see Figure 2c). Using ferrocene-tagged peptides, redox-SAMs exhibiting quantum capacitance that control the kinetics of the redox reaction at the interface in a diffusionless setting can be obtained.[32−34] These redox-tagged peptide SAMs contain terminal amino acids linked to ferrocenes by a carboxylic acid group, and similar to other SAMs, the influence of pH on the redox reaction dynamics can be expected, as shown in previous studies.[31] Hence, the evaluation of the dissociation constant of this type of redox-tagged peptide SAM permits the analysis of potential gradient shifts ($-e\Delta V$ of eq 2) and interactions between Fc−COOH and redox-active moieties in the SAM (Figure 2b). The acid dissociation of carboxylic groups of the redox-SAM and Fc−COOH in solution significantly contributes to the ET dynamics, which can be analyzed in detail through the premises of quantum-rate theory and by evaluating the energy alignment of redox moieties with the redox-SAM and the free redox moieties in the electrolyte, as it is influenced by the deprotonation of Fc−COOH that governs the efficacy of this C_q-mediated redox reaction.

This study aimed to examine the electrostatic effects of deprotonated species−interface interactions, particularly their influence on the energy level alignment and accessibility of conductive quantum channels for diffusionless ET reactions. The ET reaction of Fc−COOH was investigated at various concentrations mediated by a ferrocene-tagged SAM. A comparison of the results with those obtained using a non-electroactive SAM with a similar chemical structure confirmed the ET mediation through capacitive states. These analyses were conducted within the framework of quantum-rate theory and demonstrated the efficacy of the theory to the detailed analysis of varying electrochemical processes because the parameters of the model facilitated the experimental assessment of the impact of external factors on ET mediation. The analysis improves the understanding of the fundamental processes involved in mediated ET processes, as it improved our understanding of long-range ET reactions in biological systems,[35,36] and provides the foundation for improving the design of sensing interfaces based on the use of C_q as a transducer signal.

EXPERIMENTAL PROCEDURES

Chemical Reagents. Aqueous solutions were prepared using Milli-Q water (Simplicity water purification system, Millipore, 18.2 MΩ cm at 25 °C). Alumina suspensions (1, 0.3, and 0.05 μm) and polishing cloths (MASTERTEX) were obtained from Buehler. Sodium hydroxide (NaOH), ethyl alcohol (CH_3CH_2OH), ferrocene-carboxylic acid (Fc−COOH), HPLC-grade acetonitrile (ACN), tetrabutylammonium perchlorate ($TBAClO_4$), boric acid (H_3BO_3), phosphoric acid (H_3PO_4), and potassium ferricyanide ($K_3[Fe(CN)_6]$) were purchased from Sigma-Aldrich. Acetic acid (CH_3COOH) and potassium ferrocyanide ($K_4[Fe(CN)_6]$) were obtained from Synth. Sulfuric acid (H_2SO_4) was purchased from Qhemis. The ferrocene-tagged peptide Fc-Glu-Ala-Ala-Cys-NH_2 and the non-redox peptide Glu-Ala-Ala-Cys-NH_2 were synthesized (Supporting Information, Section SI.2) via a solid-phase peptide strategy using the Fmoc strategy on a Rink amide resin (0.5 mmol g^{-1}), as described previously.[33] The chemical structures of both peptides differed only in the ferrocene molecule.

Electrode Surface Preparation. The surface of the 2 mm diameter gold electrodes from METROHM (geometric area of 0.03142 cm^2) was cleaned as described in a previous study.[37] The electroactive interfaces were fabricated via the self-assembly of Glu-Ala-Ala-Cys-NH_2 or Fc-Glu-Ala-Ala-Cys-NH_2 to form monolayers of the non-redox peptide (pep-SAM) and redox peptide (pep-rSAM), respectively. Prior to assembly, the electrode surfaces were mechanically polished using a MASTERTEX polishing cloth and aluminum suspensions with decreasing particle sizes (1, 0.3, and 0.05 μm). Sonication in water was performed for 5 min between the polishing steps to remove adhered particles. Subsequently, the electrodes were electrochemically cleaned using cyclic voltammetry (CV) in 0.5 M NaOH with potentials ranging from −1.5 to −0.5 V (versus AglAgCl, 3 M KCl) over 200 cycles at a scan rate s of 100 mV s^{-1}, followed by water rinsing and immersion in ethanol with magnetic stirring for 20 min.

https://doi.org/10.1021/acselectrochem.4c00112
ACS Electrochem. 2025, 1, 832−841

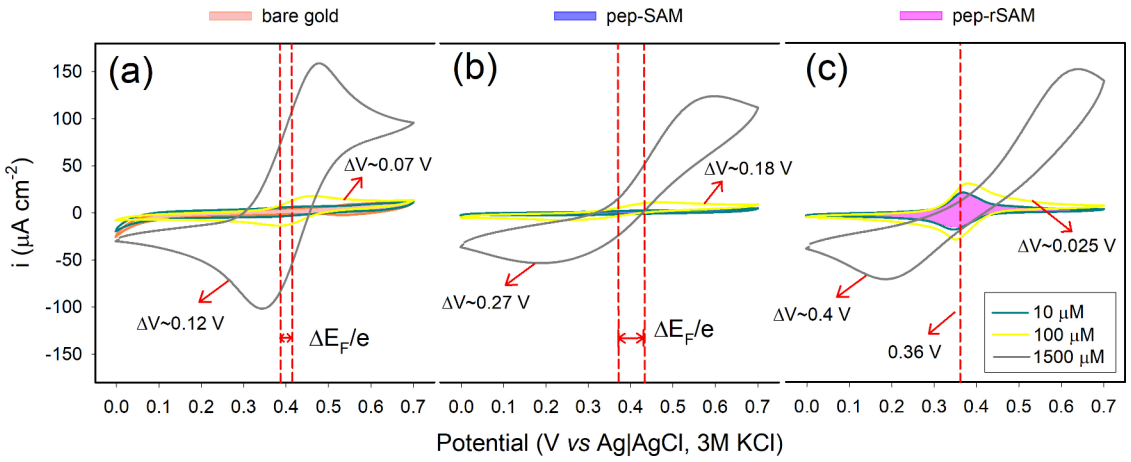

Figure 3. Representative cyclic voltammetry of 10, 100, and 1500 μM Fc−COOH in ACN/H_2O (1:4, v/v) using bare gold electrode (a), non-electroactive pep-SAM (b), and electroactive pep-rSAM (c). The peak-to-peak ΔV separation values are indicated for 100 and 1500 μM Fc−COOH for bare gold, pep-SAM, and pep-rSAM. The red dashed vertical lines show the formal potential shifts ($\Delta E_F/e$). A single value of $E_F/e \sim 0.36$ V is obtained for [Fc−COOH] < 600 μM (see Figure S12). The significant changes in peak current density after the gold electrode was modified using non-redox (b) or redox molecules (c), particularly at the highest concentration of 1500 μM. These changes are observed in Figure 4a.

Thereafter, the electrodes were electrochemically polished using CV in 0.5 M H_2SO_4 with potentials scanned from −0.2 to 1.5 V (versus AgIAgCl, 3 M KCl) for 25 cycles at a scan rate of 100 mV s^{-1}.

The mean electroactive surface areas of pep-SAM (0.045 ± 0.001 cm^2) and pep-rSAM (0.042 ± 0.003 cm^2) were calculated after a sulfuric acid cleaning step.[38] The electroactive surface area was measured by integrating the cathodic peak in the last CV electrochemical scan, using a value of 410 $\mu C\ cm^{-2}$.[38] The surface roughness was determined by dividing the electroactive area by the geometric area. This was maintained as the minimum quality control of the surface for surface roughness values of less than 1.7. The electroactive surface area values were used to calculate the current density and capacitance per unit area.

After the sulfuric acid cleaning step, the electrodes were rinsed with water and dried in a nitrogen environment. They were then immersed for 16 h at room temperature (25 °C) in 2 mM non-redox peptide or 2 mM redox peptide in 1:1 H_2O/ACN (v/v) to form SAMs over mechanically and electrochemically polished gold electrodes. The modified surfaces were rinsed with 1:1 H_2O/ACN, as described in a previous study.[37]

Electrochemical Measurements. Electrochemical analyses were performed using an AUTOLAB potentiostat (from METROHM) controlled by NOVA software. The measurements were performed using a three-electrode setup comprising a platinum mesh as the counter electrode, AgI AgCl (3 M KCl) as the reference electrode (all potentials reported in this work were measured with respect to this reference), a modified gold electrode as the working electrode, and 20 mM $TBAClO_4$ as the supporting electrolyte in ACN/H_2O (1:4, v/v) at room temperature (25 °C).

The electrochemical response of Fc−COOH at varying concentrations of [Fc−COOH] was assessed using bare and modified electrodes with peptide monolayers containing electroactive (pep-rSAM) or non-electroactive (pep-SAM) characteristics. A stock solution of 1500 μM Fc−COOH was prepared in 20 mM $TBAClO_4$ in ACN/H_2O (1:4, v/v). Serial dilutions were subsequently performed using 20 mM $TBAClO_4$ in ACN/H_2O (1:4, v/v) as the diluent, resulting in Fc−COOH aliquots with concentrations ranging from 1 to 1500 μM Fc−COOH.

CVs were recorded from 0.0 to 0.7 V (three cycles) at a scan rate of 100 mV s^{-1} using either the unmodified or modified electrode. The formal potentials of the Fc−COOH (E_F^e/e) and the redox-SAM (E_F^m/e) were measured as $E_F/e \sim (V_{ox} + V_{red})/2$, where V_{ox} and V_{red} are the oxidation and reduction potential peaks of the corresponding CV, respectively. Subsequently, EIS was conducted at E_F/e using the FRA module of AUTOLAB. The frequencies ranged from 100 kHz to 0.1 Hz (total of 60 logarithmically arranged frequencies with a sinusoidal potential perturbation RMS amplitude of 10 mV). For redox-SAM, additional EIS measurement was conducted at a potential outside the faradaic window, which was referred to as $V_{out} \sim 0.1$ V.

Electrochemical capacitance spectroscopy (ECS) spectra were constructed using a complex capacitance function $C^*(\omega) = 1/j\omega Z^*(\omega)$ from the EIS raw data $Z^*(\omega)$, where j is the complex number $j = \sqrt{-1}$, ω is the angular frequency $\omega = 2\pi f$, and f is the linear frequency.[2,39,40] The capacitance complex function facilitates the determination of the capacitance spectra by using $C^*(\omega) = C' + jC''$, where C' and C'' are the real and imaginary capacitive components, respectively. These values are calculated using the mathematical equations $C' = \phi Z''$ and $C'' = \phi Z'$, where Z' and Z'' are the real and imaginary impedance components, respectively, and $\phi = 1/(\omega|Z|^2)$, in which $|Z|$ is the modulus of the impedance.

The values of the circuit elements were obtained by fitting EIS to appropriate equivalent circuit models of the interface (Figures S7, S11, and S16). The values of the equivalent circuit elements obtained from the fitting are stated as the mean value $\bar{x}$ with the standard error of the mean $\sigma_{\bar{x}}$ ($\bar{x} \pm \sigma_{\bar{x}}$) calculated for two (pep-SAM) and three (pep-rSAM) independently fabricated interfaces.

Determination of pK_a. The pK_a values of Fc−COOH, pep-SAM, and pep-rSAM were determined by differential pulse voltammetry (DPV) using the same three-electrode cell, as described previously. The measurements were conducted in Britton−Robinson buffer solutions. The potential sweep in

https://doi.org/10.1021/acselectrochem.4c00112
ACS Electrochem. 2025, 1, 832−841

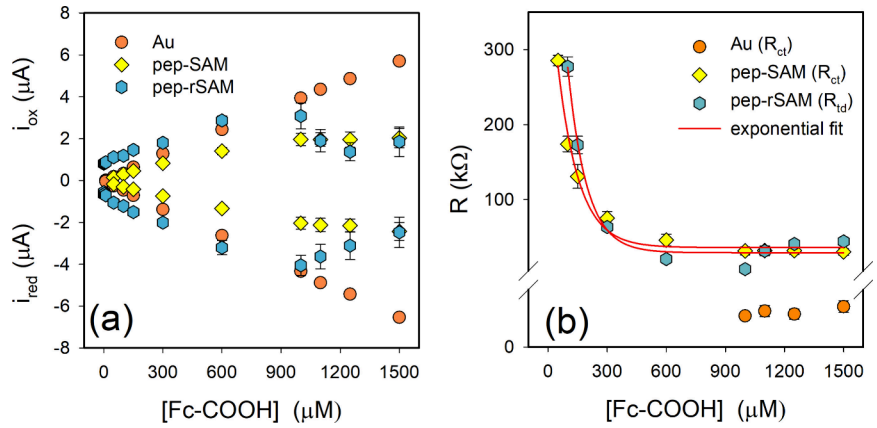

Figure 4. Peak current (a) and resistance values (b) as a function of Fc−COOH concentration for three systems: the unmodified gold electrode (Au), the non-electroactive pep-SAM, and the electroactive pep-rSAM. In (b), R_{ct} is used for Au and pep-SAM, whereas R_{td} is used for pep-rSAM. Exponential decay regressions with good fit ($r^2 > 0.98$) indicate that the resistance decreased with increasing Fc−COOH concentration for pep-SAM and pep-rSAM. The R_{ct} values of the unmodified gold electrode (Au) at low Fc−COOH concentrations (not shown) were statistically inaccurate.

anodic and cathodic directions (potential range for Fc−COOH from 0 to 0.7 V, and for the monolayers from −0.2 to 0.7 V) was performed at a pulsed potential (70 mV) during short pulses (70 ms). In addition, ECS was used for the pK_a calculation of pep-rSAM, wherein EIS was performed on the same buffer solutions at E_F/e calculated using the DPV profiles.

Britton−Robinson buffers (pH = 3 to 8.3) were prepared by modifying 20 mM $TBAClO_4$ in an ACN/H_2O (1:4, v/v) solution. Buffered electrolyte solutions were prepared from an equal mixture of 0.04 M CH_3COOH, 0.04 M H_3BO_3, and 0.04 M H_3PO_4.[41] The pH value was adjusted using 0.2 M NaOH. The pH values of the buffer solutions were measured by using a pH meter equipped with a glass electrode (Sensoglass). To determine the pK_a of Fc−COOH, buffer solutions were prepared with 100 μM Fc−COOH, whereas a ferricyanide/ferrocyanide redox couple (2 mM $[Fe(CN)_6]^{3-/4-}$) was used as the electroactive species in the buffer preparation for the determination of the pK_a for pep-SAM. Regarding pep-rSAM, Britton−Robinson buffers containing the non-redox probe was used.

RESULTS AND DISCUSSION

Effects of Fc−COOH Concentration on the Diffusion-Controlled ET in the Fc−COOH/Electrode Interface. The ET between ferrocene/ferrocenium (Fc−COOH/Fc^+−COOH) carboxylic acid species and the unmodified gold electrode is governed by diffusion-controlled ET, as confirmed and detailed in Section SI.4. The ET reaction was reversible for concentrations between 50 and 600 μM (see Figure S5), as confirmed by the peak-to-peak separation $\Delta V < 90$ mV and peak current ratio $i_{ox}/i_{red} \sim 1$, in agreement with the expected behavior.[1] Figure 3a shows the representative CVs of varying Fc−COOH concentrations, where the faradaic current surpassed the non-faradaic current (attributed to the double layer capacitance) as the [Fc−COOH] increased during the diffusion-controlled redox reaction, resulting in a formal potential of $E_F^e/e \sim 0.36$ V. At higher [Fc−COOH], E_F^e/e shifted toward higher potentials (approximately 0.42 V), implying that the redox reaction required a higher potential to occur.

The observed shift in the formal potential toward higher values at [Fc−COOH] > 1000 μM was attributed to the accumulation of negatively charged Fc−COO^-/Fc^+−COO^- species near the electrode surface. This electrostatic repulsion hindered the approach of incoming molecules, thus requiring a higher potential for ET to occur. The deprotonation of Fc−COOH to Fc−COO^- was caused by the pH of the supporting electrolyte solution (ca. 6.67), which was higher than the pK_a of Fc−COOH (ca. 5.47 ± 0.03; see Section SI.3). This pK_a is also higher than that reported by Fabbrizzi et al.[23] owing to the distinct solvent environment, hindering the observation of the acid region for a redox reaction that is pH-dependent, as expected from Pourbaix diagrams analysis; see Section SI.3 for more details.

Therefore, the PCET reaction for Fc−COOH in this study involved the ET of ferrocene after the transfer of H^+ to the aqueous solvent. The ET reaction between Fc−COO^-/Fc^+−COO^- and the metallic electrode (*electrode*) is described by Fc−COO^- ⇌ Fc^+−COO^- + e^- (*electrode*). At high concentrations, the diffusion layer (formed around the electrode) may become saturated with charged species, limiting the rate at which fresh Fc−COO^-/Fc^+−COO^- molecules reach the surface, which affects the values of R_{ct} obtained by fitting the EIS measurement using the equivalent circuit shown in Figure S7, which increased as [Fc−COOH] increased (Table S2). Hence, a higher potential was required to promote the ET reaction.

Surface Charge Effects of pep-SAM on the Diffusion-Controlled ET Dynamics in the Fc−COOH/pep-SAM/Electrode Interface. The non-electroactive (dielectric) pep-SAM significantly, as expected, hindered the reversible behavior of Fc−COOH at the gold electrode, acting as a blocking layer for the ET reaction. The CV profiles in Figure 3b exhibited deviations from the reversibility with $\Delta V > 180$ mV and $i_{ox}/i_{red} \neq 1$ (see Figure S8). This indicated that unequal concentrations of oxidized and reduced species were present at the electrode surface, leading to reduced and unbalanced anodic and cathodic currents compared to those at the unmodified electrode (see Figure 3a).

At concentrations lower than 10 μM, the faradaic current did not surpass the non-faradaic capacitance of pep-SAM (depicted by the blue shadow CV in the inset of Figure S8). However, the calculated values of $i_{ox}/i_{red} \neq 1$ for concentrations higher than 50 μM suggest that reduction reactions were

https://doi.org/10.1021/acselectrochem.4c00112
ACS Electrochem. 2025, 1, 832−841

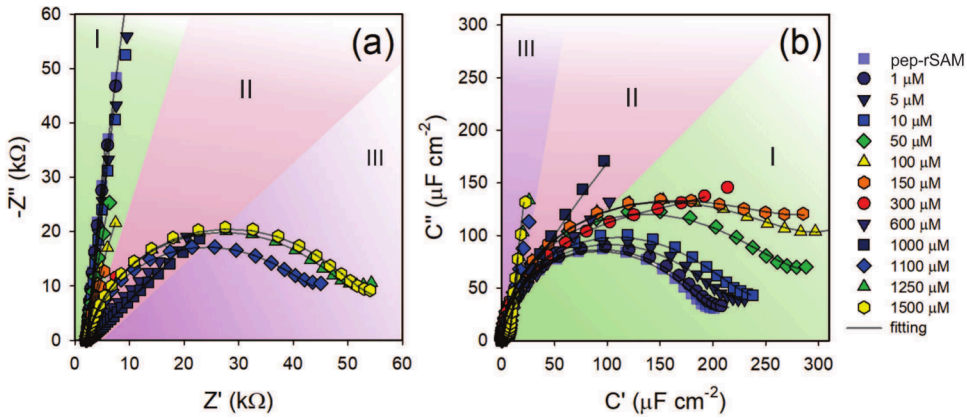

Figure 5. Complex impedance (a) and capacitance (b) Nyquist plots of the redox monolayer, pep-rSAM, at varying Fc−COOH concentrations in ACN/H_2O (1:4, v/v). Each plot can be divided into three regions based on the dominant electrochemical behavior: (I) quantum capacitive dominance; (II) intermediate or transition region; and (III) resistive dominance.

favored over oxidative reactions. Because pep-SAM is negatively charged at pH 6.67, its pK_a value was approximately 5.15 (Figure S9); neutral Fc^+−COO^- species experience less electrostatic repulsion by negatively charged pep-SAM, in comparison to charged Fc−COO^-, potentially contributing to the observed preference for the reduction reaction.

The impedance data (Figure S10) confirmed the non-faradaic capacitance values observed in Figure 3, with minimal changes in the response owing to the increase in [Fc−COOH]. An exponential reduction of the R_{ct} obtained using equivalent circuit fitting (Figure S11) was observed with increasing values of [Fc−COOH] (Figure 4b). This trend coincides with the increase in the peak currents observed in Figure 4a for [Fc−COOH] < 1000 μM. Thus, for concentration higher than 1000 μM, the electrostatic repulsion hinders the proximity of the redox probe to the surface.

The R_{ct} values obtained in the presence of pep-SAM were significantly higher (1000-fold) than those obtained using a bare gold electrode (see Figure 4b), highlighting the insulating (or dielectric) character of the non-redox peptide monolayer.

Because of the absence of redox states in the molecular structure of this monolayer, the non-electroactive pep-SAM did not exhibit quantum state levels (e.g., C_q) for charge, although the ET between Fc−COO^-/Fc^+−COO^- and the electrode transpired following the quantum mechanical tunneling processes operating at the nanoscale thickness of this SAM, as described in a previous study.[42] The following section discusses the results obtained using a different type of SAM (pep-rSAM), which features a ferrocene molecule incorporated into the peptide structure to produce a redox-active monolayer that exhibits a different (diffusionless) ET mechanism, as reported in a previous study.[10]

Diffusionless ET Dynamics on Fc−COOH/pep-rSAM/Electrode Interface: The Effect of Fc−COOH Concentration. Compared with the blocking effect observed for pep-SAM, redox-SAMs with C_q states provide a promising approach for suppressing electrostatic barriers, supplying quantum channels for mediating the ET reaction with quantum resistance (R_q ~ 12.9 kΩ).[9] Expanding on previous studies exploring the mediation of ET between the electrode and redox species by redox-SAMs,[a] the robustness of this approach was assessed based on the alignment of energy levels studied across a wider concentration range.

Because the pH of the supporting electrolyte (6.67) was higher than the pK_a of pep-rSAM (~4.5, see Figure S15), ionizable protons of the redox-active pep-rSAM were transferred to the solvent, creating a negatively charged surface. The well-known electroactive response of pep-rSAM was observed at 0.365 V (Figure S12). Because of the charged surface arising from the PCET of pep-rSAM, the ET mediation of Fc−COO^-/Fc^+−COO^- in solution was significantly affected (see Figure S12). Formal potential shifts from 0.36 to 0.42 V with increasing [Fc−COOH] were observed. This resulted in non-reversible behavior at saturated concentrations, as shown in Figure 3c.

Although the CV shown in Figure S12 suggests that a coupled ET process occurred between the tethered Fc in pep-rSAM and free Fc−COO^-/Fc^+−COO^-, the overall electrochemical response depended on [Fc−COOH]. The reversible behavior (ΔV < 90 mV, i_{ox}/i_{red} ~ 1) was maintained up to 600 μM and accompanied by an increase in the faradaic current compared with direct ET using the bare electrode (Figure 4a). Because the electrochemical faradaic current is related to the quantum capacitance by the scan rate s as $i = C_q s$,[8] and $C_q \propto N$ (eq 1), the enhancement of i was attributed to the quantum states N of pep-rSAM, which were enabled by the sustained energy level alignment (E_F^m/e ~ 0.365 V).

The linear increase in faradaic current as a function of [Fc−COOH] observed between 1 and 600 μM deviated significantly at higher concentrations (≥1000 μM) and was associated with a significant reduction in the faradaic current (Figure 4a). This reduction was likely due to the surface charge of pep-rSAM, which can repel the negatively charged Fc−COO^- species, hindering their access to the electrode surface and thereby limiting ET efficiency. Further discussion of these electrostatic interactions is provided in the following section.

ET Efficiency between Fc−COOH and pep-rSAM: Potential Gradient Effects. The negatively charged surface of pep-rSAM did not affect ET mediation via the C_q states for [Fc−COOH] ≤ 600 μM, facilitating the approach of Fc−COO^-/Fc^+−COO^- to the interface for the redox reaction without affecting the ET dynamics (Figure 6a). However, at higher concentrations (≥1000 μM), the response deviated from equilibrium (ΔV > 120 mV, i_{ox}/i_{red} < 0.8), suggesting limitations in ET efficiency. Although Fc^+−COO^- approached the surface for reduction, the change in the equilibrium Fc−COO^- ⇌ Fc^+−COO^- + e^- (*monolayer*) to the reverse

https://doi.org/10.1021/acselectrochem.4c00112
ACS Electrochem. 2025, 1, 832−841

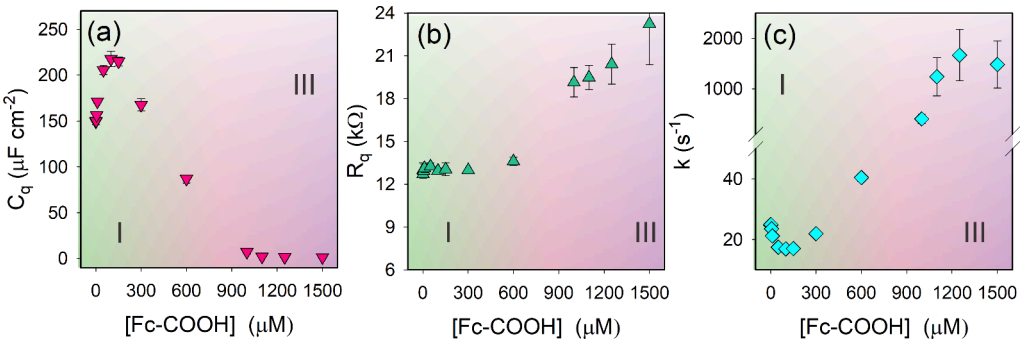

Figure 6. Behavior of quantum capacitance C_q (a) and quantum resistance R_q (b), which ultimately affect ET kinetics k (c) based on the Fc−COOH concentration. An exponential increase in C_q results in ET following the quantized resistance limit, where R_q remains constant at approximately 12.9 kΩ within experimental error. In region I (a), the negatively charged surface of pep-rSAM facilitated the approach of the Fc−COO$^-$/Fc$^+$−COO$^-$ species to the monolayer for ET with quantized efficiency; therefore, this process occurred with minimum resistance, R_q. However, in region III (b), the saturation of the interface with these species results in electrostatic repulsion with the negative charge. This disrupts the C_q states, hinders ET, and promotes reduction over oxidation.

reaction likely coincided with changes in the C_q state occupation owing to the surface charge repulsion of Fc−COO$^-$ (see Figure 7b).

The Nyquist diagrams (Figure 5) confirm the initial increase and subsequent reduction in C_q with increasing [Fc−COOH]. Three regions were observed: region I, low [Fc−COOH] with dominant capacitance and increasing C_q (Figure 5b); region II, an intermediate region with reduced capacitive dominance; and region III, high [Fc−COOH] with high impedance (Figure 5a). A capacitive contribution was observed even at high concentrations; however, this contribution was not dominant (Table S10).

C_q values from the fitting (Table S10) aligned with this behavior. Figure 6a shows the initial increase in C_q from approximately 149 to 215 μF cm^{-2} within region I. The increase in available N states that can mediate the ET reaction of the Fc−COO$^-$/Fc$^+$−COO$^-$ species approaching the pep-rSAM surface (Figure 7a) resulted in an increase in the faradaic current (Figure 4a). For region I, the calculation[b] of R_q (Table S10) confirms that quantum states mediate the ET between the Fc−COOH in solution and the electrode because the observed resistance value was within the quantum limit (ca. 12.9 kΩ) (see Figure 6b). Because C_q and R_q govern the ET kinetics with quantum efficiency in region I, the ET rates obtained by employing the quantum-rate expression $k = 4e^2/hC_q$ (eq S5) can be observed when ET is or is not mediated by the C_q states (Figure 6c).

In region III ([Fc−COOH] ≥ 1000 μM), saturation with Fc−COO$^-$/Fc$^+$−COO$^-$ species resulted in electrostatic repulsion with the negatively charged monolayer (Figure 7b), modifying the C_q state occupation, which resulted in a 21-fold reduction in capacitance (Figure 6a). Consequently, no N states were available for ET mediation. This hindered the accessibility extended to the C_q states of pep-rSAM, suggesting energy level changes and loss of the previously observed alignment, shifting E_F^m/e from 0.36 to 0.42 V. For instance, at 1500 μM, a non-reversible CV was obtained, as shown in Figure 3c. For region III, the obtained R_q values were not within the quantum limit (>19 kΩ), suggesting that the previous efficiency was not attained (see Table S10). Therefore, the absence of quantum circuit elements governing the ET rate leads to a constant rate different from that obtained in region I, likely reflecting the high energy barrier that the ET process must overcome for tunneling when the quantum states are no longer involved in the intermediation of the ET process.

R_{td} is used in the equivalent circuit description to model the parallel ET paths that constitute the ET process without mediation[10] by C_q states of the interface. The trend of R_{td} values as a function of [Fc−COOH] was similar to that of the R_{ct} of pep-SAM (lacking C_q states), as shown in Figure 4b. This confirmed that the parallel ET transfer process was not mediated by the C_q states. The high values of R_{td}, which exceeded those of R_q, indicate a significant energy cost for ET to occur via this type of ET path.

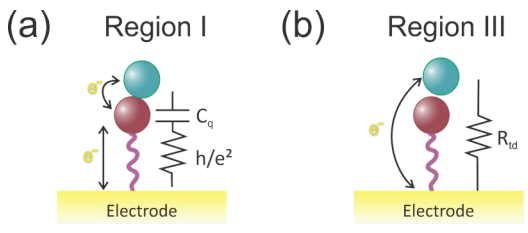

Figure 7. Schematic illustration of the potential gradient effect on the diffusionless ET dynamics mediated by C_q states within pep-rSAM. (a) Enhanced ET reaction occurring in the region I of Nyquist diagrams (see Figure 5), where there is quantum RC dynamics governing the ET reaction. (b) Hindered ET reaction due to the high concentration of negatively charged redox species in region III, leading to electrostatic repulsion between charges within redox species in the SAM and free moieties in the electrolytic medium. The occupancy of C_q states is altered as a result of these charging effects, affecting the ET-mediated reaction with a perceptible charge in R_{td} parallel ET and diffusion-dependent ET process (see Figure S16).

FINAL REMARKS AND CONCLUSIONS

This study demonstrates that electrostatic interactions are crucial in tuning ET reactions mediated by C_q states. By modulating the acidity of the SAM and free redox species in the electrolyte, one can either enhance or hinder the efficiency of the mediated ET. At high concentrations of negatively charged redox species, the electrostatic repulsion between Fc−COO$^-$ and the negatively charged pep-rSAM surface shifts the formal potential, disrupting energy level alignment and hindering effective ET mediation. Further analysis using density functional theory simulations, for instance, of this energy level alignment can provide insight into the resultant

https://doi.org/10.1021/acselectrochem.4c00112
ACS Electrochem. 2025, 1, 832−841

HOMO−LUMO energy gap of the interaction between the negatively charged redox-SAM with both Fc−COO^- (negatively charged) and Fc^+−COO^- (neutral species).

Quantum RC dynamics where C_q and R_q govern the ET dynamics implies additional quantum channels N available, which is computed as an increase in C_q of the interface. This quantum RC dynamics with increasing $E = e^2/C_q$ results in an enhanced flow of electrons as contributions from both redox-SAM and free redox species in solution. This acidity equilibrium between redox species in the SAM and those free in solution influences the mediation of ET by affecting the acidity and the potential gradient ΔV (eq 2), which ultimately affects the occupancy and energy alignment between the quantum states in the SAM and the free redox species in the electrolyte environment. Our findings highlight the importance of considering these effects (electrostatics driven by protonation/deprotonation) in designing C_q-mediated ET interfaces, which has significant implications in designing sensing interfaces. For the design of these sensing interfaces, carefully considering how the chemistry influences the physical properties of the interface is important, as it must be monitored and taken into account.

■ ASSOCIATED CONTENT

Supporting Information

The Supporting Information is available free of charge at https://pubs.acs.org/doi/10.1021/acselectrochem.4c00112.

Quantum-rate theory, peptide characterization, additional electrochemical characterization, and additional equivalent circuit analysis (PDF)

■ AUTHOR INFORMATION

Corresponding Author

Paulo Roberto Bueno − *Institute of Chemistry, São Paulo State University (UNESP), Araraquara, São Paulo 14800-060, Brazil;* orcid.org/0000-0003-2827-0208; Email: paulo-roberto.bueno@unesp.br

Authors

Yuliana Pérez Sánchez − *Institute of Chemistry, São Paulo State University (UNESP), Araraquara, São Paulo 14800-060, Brazil*

Adriano dos Santos − *Institute of Chemistry, São Paulo State University (UNESP), Araraquara, São Paulo 14800-060, Brazil;* orcid.org/0000-0001-6812-5609

Complete contact information is available at: https://pubs.acs.org/10.1021/acselectrochem.4c00112

Author Contributions

Y.P.S. contributed to the conceptualization, experimental design, performed the electrochemical data collection, data analysis and interpretation, investigation, formal analysis, designed the schematic illustrations, and wrote the manuscript. A.d.S. contributed to the experimental design and interpretation and reviewed the manuscript. P.R.B. contributed to the conceptualization, experimental design and interpretation, funding acquisition, project administration, supervision, data curation, resources, and wrote the manuscript.

Funding

This work has been supported by the São Paulo State Research Foundation (FAPESP, grant nos. 2017/24839-0, 2024/02000-2, and 2023/15384-0) and the National Council for Scientific and Technological Development (CNPq, 305582/2023-2), Brazil. The Article Processing Charge for the publication of this research was funded by the Coordenacao de Aperfeicoamento de Pessoal de Nivel Superior (CAPES), Brazil (ROR identifier: 00x0ma614).

Notes

The authors declare no competing financial interest.

■ ACKNOWLEDGMENTS

We thank Professor Eduardo M. Cilli for his help with the synthesis of the self-assembled peptides used in this study.

■ ADDITIONAL NOTES

[a]This is achieved by the energy level alignment of non-capacitive (redox species) and the quantum capacitive states (redox moieties in the electroactive SAM), focusing on a single 100 μM Fc−COOH.[10]

[b]R_q was measured as the total contribution of series resistance comprising R_s and the monolayer resistance R_{qt} obtained from the equivalent circuit fitting (Figure S16), as described previously.[9]

■ REFERENCES

(1) Bard, A. J.; Faulkner, L. R. In *Electrochemical Methods Fundamentals and applications*, 2nd ed.; John Wiley and Sons, 2000.

(2) Bueno, P. R. In *The Nanoscale Electrochemistry of Molecular Contacts*; SpringerBriefs in Applied Sciences and Technology; Springer, 2018.

(3) Bueno, P. R. Quantum rate theory and electron-transfer dynamics: A theoretical and experimental approach for quantum electrochemistry. *Electrochimica Acta* **2023**, *466*, 142950.

(4) Laviron, E. General expression of the linear potential sweep voltammogram in the case of diffusionless electrochemical systems. *Journal of Electroanalytical Chemistry* **1979**, *101*, 19−28.

(5) Chidsey, C. E. D. Free-energy and temperature-dependence of electron-transfer at the metal-electrolyte interface. *Science* **1991**, *251*, 919−922.

(6) Lopes, L. C.; Pinzón, E. F.; Dias-da Silva, G.; Feliciano, G. T.; Bueno, P. R. Electrochemical measurement of the electronic structure of graphene via quantum mechanical rate spectroscopy. *Electrochimica Acta* **2024**, *480*, 143837.

(7) Pinzón, E. F.; Lopes, L. C.; Fonseca, A. F. V.; Schiavon, M. A.; Bueno, P. R. Quantum rate as a spectroscopic methodology for measuring the electronic structure of quantum dots. *Journal of Materials Chemistry C* **2024**, *12*, 4606−4617.

(8) Alarcón, E. V. G.; Santos, A.; Bueno, P. R. Perspective on Quantum Electrochemistry. A Simple Method for Measuring the Electron Transfer Rate Constant. *Electrochimica Acta* **2021**, *398*, 139219.

(9) Sanchez, Y. P.; Santos, A.; Bueno, P. R. Quantum Mechanical Meaning of the Charge Transfer Resistance. *J. Phys. Chem. C* **2022**, *126*, 3151−3162.

(10) Sánchez, Y. P.; Santos, A.; Roberto Bueno, P. Quantum rate efficiency of the charge transfer mediated by quantum capacitive states. *Electrochimica Acta* **2022**, *434*, 141194.

(11) Li, J.; Schuler, K.; Creager, S. E. A Generalized Equivalent-Circuit Model for Electroactive Monolayers Exhibiting a Fixed Redox Potential and a Distribution of Electron-Transfer Rate Constants I. Square Distributions. *J. Electrochem. Soc.* **2000**, *147*, 4584.

(12) Moreira, T. F.; Pinzón, E. F.; Santos, A. d.; Lopes, L. C.; Bueno, P. R. The quantum mechanical origin of the supercapacitance phenomenon in reduced graphene oxide structures. *Carbon* **2025**, *232*, 119736.

(13) Bueno, P. R.; Feliciano, G. T.; Davis, J. J. Capacitance spectroscopy and density functional theory. *Physical Chemistry Chemical Physics* **2015**, *17*, 9375−9382.

(14) Bueno, P. R.; Cruzeiro, V. W.; Roitberg, A. E.; Feliciano, G. T. The density-of-States and equilibrium charge dynamics of redox-active switches. *Electrochimica Acta* **2021**, *387*, 138410.
(15) Pinzón Nieto, E.; Alarcón, E. V. G.; Sánchez, Y. P.; Bueno, P. R. Quantum Rate Dynamics and Charge Screening at the Nanoscale Level. *Phys. Chem. Chem. Phys.* **2022**, *24*, 16200.
(16) Reiss, H. The Fermi level and the redox potential. *J. Phys. Chem.* **1985**, *89*, 3783−3791.
(17) Macdonald, J. R.; Johnson, W. B.; Raistrick, I. D.; Franceschetti, D. R.; Wagner, N.; McKubre, M. C. H.; Macdonald, D. D.; Sayers, B.; Bonanos, N.; Steele, B. C. H.; et al. In *Impedance spectroscopy: theory, experiment, and applications*; John Wiley & Sons, 2018.
(18) Miranda, D. A.; Bueno, P. R. Density functional theory and an experimentally-designed energy functional of electron density. *Physical Chemistry Chemical Physics* **2016**, *18*, 25984−25992.
(19) Garrote, B. L.; Santos, A.; Bueno, P. R. Perspectives on and precautions for the uses of electric spectroscopic methods in label-free biosensing applications. *ACS sensors* **2019**, *4*, 2216−2227.
(20) Forster, R. J.; Faulkner, L. R. Electrochemistry of spontaneously adsorbed monolayers. Effects of solvent, potential, and temperature on electron transfer dynamics. *J. Am. Chem. Soc.* **1994**, *116*, 5453−5461.
(21) Finklea, H. O.; Ravenscroft, M. S.; Snider, D. A. Electrolyte and temperature effects on long range electron transfer across self-assembled monolayers. *Langmuir* **1993**, *9*, 223−227.
(22) Zhu, G. Y.; Qin, Y.; Meng, M.; Mallick, S.; Gao, H.; Chen, X.; Cheng, T.; Tan, Y. N.; Xiao, X.; Han, M. J.; Sun, M. F.; Liu, C. Y. Crossover between the adiabatic and nonadiabatic electron transfer limits in the Landau-Zener model. *Nat. Commun.* **2021**, *12*, 456.
(23) De Santis, G.; Fabbrizzi, L.; Licchelli, M.; Pallavicini, P. Controlling the acidity of the carboxylic group by a ferrocene based redox switch. *Inorganica chimica acta* **1994**, *225*, 239−244.
(24) Molinero, V.; Calvo, E. J. Electrostatic interactions at self assembled molecular films of charged thiols on gold. *Journal of electroanalytical chemistry* **1998**, *445*, 17−25.
(25) Beulen, M. J.; van Veggel, F. J.; Reinhoudt, D. Coupling of acid−base and redox functions in mixed sulfide monolayers on gold. *Chem. Commun.* **1999**, *6*, 503−504.
(26) Del Caño, R.; Mateus, L.; Sánchez-Obrero, G.; Manuel Sevilla, J.; Madueño, R.; Blázquez, M.; Pineda, T. Hemoglobin becomes electroactive upon interaction with surface-protected Au nanoparticles. *Talanta* **2018**, *176*, 667−673.
(27) Márquez, I.; Olloqui-Sariego, J. L.; Molero, M.; Andreu, R.; Roldán, E.; Calvente, J. J. Active Role of the Buffer in the Proton-Coupled Electron Transfer of Immobilized Iron Porphyrins. *Inorg. Chem.* **2021**, *60*, 42−54.
(28) Tan, K.-J.; Morikawa, S.; Ozbek, N.; Lenz, M.; Arlt, C.-R.; Tschope, A.; Franzreb, M.; Hatton, T. A. Redox Polyelectrolytes with pH-Sensitive Electroactive Functionality in Aqueous Media. *Langmuir* **2023**, *39*, 2943−2956.
(29) Mayer, J. M. Proton coupled electron transfer: a reaction chemist's view. *Annual Review of Physical Chemistry* **2004**, *55*, 363−390.
(30) McCarthy, B. D.; Dempsey, J. L. Decoding proton coupled electron transfer with potential pKa diagrams. *Inorg. Chem.* **2017**, *56*, 1225−1231.
(31) Costentin, C.; Robert, M.; Savéant, J.-M. Update 1 of: Electrochemical approach to the mechanistic study of proton-coupled electron transfer. *Chem. Rev.* **2010**, *110*, PR1−PR40.
(32) Piccoli, J. P.; Santos, A.; Santos-Filho, N. A.; Lorenzon, E. N.; Cilli, E. M.; Bueno, P. R. The self-assembly of redox active peptides: Synthesis and electrochemical capacitive behavior. *Peptide Science* **2016**, *106*, 357−367.
(33) Piccoli, J.; Hein, R.; El-Sagheer, A. H.; Brown, T.; Cilli, E. M.; Bueno, P. R.; Davis, J. J. Redox Capacitive Assaying of C-Reactive Protein at a Peptide Supported Aptamer Interface. *Analytical Chemistry* **2018**, *90*, 3005−3008.
(34) Brandão, S. T. R.; dos Santos, A.; Bueno, P. R.; Cilli, E. M. Designing Quantum Capacitive Peptide Interfaces for Electro-analytical Applications. *Analytical Chemistry* **2023**, *95*, 13470−13477.
(35) Migliore, A.; Polizzi, N. F.; Therien, M. J.; Beratan, D. N. Biochemistry and theory of proton-coupled electron transfer. *Chem. Rev.* **2014**, *114*, 3381−3465.
(36) Kaila, V. R. Resolving chemical dynamics in biological energy conversion: Long-range proton-coupled electron transfer in respiratory complex I. *Acc. Chem. Res.* **2021**, *54*, 4462−4473.
(37) Garrote, B. L.; Santos, A.; Bueno, P. R. Label-free capacitive assaying of biomarkers for molecular diagnostics. *Nat. Protoc.* **2020**, *15*, 3879.
(38) Trasatti, S.; Petrii, O.A. Real surface-area measurements in electrochemistry. *Electrochimica Acta* **1992**, *327*, 353−376.
(39) Bueno, P. R.; Benites, T. A.; Davis, J. J. The Mesoscopic Electrochemistry of Molecular Junctions. *Sci. Rep.* **2016**, *6*, 18400.
(40) Bueno, P. R.; Mizzon, G.; Davis, J. J. Capacitance spectroscopy: A versatile approach to resolving the redox density of states and kinetics in redox-active self-assembled monolayers. *J. Phys. Chem. B* **2012**, *116*, 8822−8829.
(41) Mongay, C.; Cerda, V. A Britton-Robinson buffer of known ionic strength. *Annali di Chimca* **1974**, *64*, 409.
(42) Finklea, H. O.; Hanshew, D. D. Electron-transfer kinetics in organized thiol monolayers with attached pentaamine (pyridine) rutheninum redox centers. *J. Am. Chem. Soc.* **1992**, *114*, 3173−3181.

https://doi.org/10.1021/acselectrochem.4c00112
ACS Electrochem. 2025, 1, 832−841